**LETTER • OPEN ACCESS**

# Greenhouse gas fluxes from reservoirs determined by watershed lithology, morphometry, and anthropogenic pressure

To cite this article: Elizabeth León-Palmero *et al* 2020 *Environ. Res. Lett.* **15** 044012

View the article online for updates and enhancements.

# Environmental Research Letters

**LETTER**

# Greenhouse gas fluxes from reservoirs determined by watershed lithology, morphometry, and anthropogenic pressure

Elizabeth León-Palmero[1] ⓘ , Rafael Morales-Baquero[1] ⓘ and Isabel Reche[1,2] ⓘ

[1] Instituto del Agua and Departamento de Ecología, Universidad de Granada, E-18071 Granada, Spain
[2] Research Unit Modeling Nature (MNat), Universidad de Granada, E-18071 Granada, Spain

**E-mail:** ireche@ugr.es

## Abstract

Human population growth has increased the demand for water and clean energy, leading to the massive construction of reservoirs. Reservoirs can emit greenhouse gases (GHG) affecting the atmospheric radiative budget. The radiative forcing due to $CO_2$, $CH_4$, and $N_2O$ emissions and the relative contribution of each GHG in terms of $CO_2$ equivalents to the total forcing is practically unknown. We determined simultaneously the $CO_2$, $CH_4$, and $N_2O$ fluxes in reservoirs from diverse watersheds and under variable human pressure to cover the vast idiosyncrasy of temperate Mediterranean reservoirs. We obtained that GHG fluxes ranged more than three orders of magnitude. The reservoirs were sources of $CO_2$ and $N_2O$ when the watershed lithology was mostly calcareous, and the crops and the urban areas dominated the landscape. By contrast, reservoirs were sinks of $CO_2$ and $N_2O$ when the watershed lithology was predominantly siliceous, and the landscape had more than 40% of forestal coverage. All reservoirs were sources of $CH_4$, and emissions were determined mostly by reservoir mean depth and water temperature. The radiative forcing was substantially higher during the stratification than during the mixing. During the stratification the radiative forcings ranged from 125 mg $CO_2$ equivalents $m^{-2} d^{-1}$ to 31 884 mg $CO_2$ equivalents $m^{-2} d^{-1}$ and were dominated by the $CH_4$ emissions; whereas during the mixing the radiative forcings ranged from 29 mg $CO_2$ equivalents $m^{-2} d^{-1}$ to 722 mg $CO_2$ equivalents $m^{-2} d^{-1}$ and were dominated by $CO_2$ emissions. The $N_2O$ contribution to the radiative forcing was minor except in one reservoir with a landscape dominated by crops and urban areas. Future construction of reservoirs should consider that siliceous bedrocks, forestal landscapes, and deep canyons could minimize their radiative forcings.

## Introduction

Human population growth has increased the need for water and clean energy, promoting the construction of reservoirs for irrigation, consumption, and hydropower. The number of reservoirs has increased significantly over the past 60 years, reaching over 16.7 million dams globally (Lehner *et al* 2011). This trend is still ongoing, especially in countries with emerging economies, where over 3000 major hydropower dams are either planned or under construction (Zarfl *et al* 2015). Now it widely is accepted that inland waters, including reservoirs, despite their small global surface area, contribute much in proportion to the global

carbon cycle (Tranvik *et al* 2009, Raymond *et al* 2013). Reservoirs have a radiative forcing dependent on their greenhouse gas (GHG) emissions (Barros *et al* 2011, Deemer *et al* 2016). The $CO_2$ emissions from inland waters (ca. 2.1 Pg C $yr^{-1}$) are similar in magnitude to the estimate of the global uptake of $CO_2$ by the global ocean (2.4 Pg C $yr^{-1}$) (Le Quéré *et al* 2018). Lakes and reservoirs are usually $CO_2$ supersaturated (Cole *et al* 1994), releasing 0.32 Pg C $yr^{-1}$ (Raymond *et al* 2013). In carbonate-poor lakes, an excess of respiration over primary production produces supersaturation, whereas, in calcareous watersheds, supersaturation is due to the loadings of inorganic carbon during the weathering (López *et al* 2011, McDonald *et al* 2013,

Marcé *et al* 2015, Weyhenmeyer *et al* 2015). Inland waters are not only sources of $CO_2$, but they can be significant sources of $CH_4$ and $N_2O$ (Tranvik *et al* 2009, Bastviken *et al* 2011, Soued *et al* 2015) with warming potential of 34 and 298 times higher than $CO_2$ in a 100 year timescale (IPCC 2013).

$CH_4$ emissions from reservoirs appear to be responsible for the majority of their radiative forcings (ca. 80% of the $CO_2$ equivalents) and are comparable to emissions from paddies or biomass burning (Deemer *et al* 2016, Samiotis *et al* 2018). Reservoirs, collectively considered, emit 13.3 Tg C $yr^{-1}$ of $CH_4$, although there is an astonishing lack of data, which severely limits our confidence in this global estimation (Deemer *et al* 2016). Methanogenesis is a microbial process more sensitive to temperature than other processes as, for instance, methanotrophy, respiration, and photosynthesis (Marotta *et al* 2014, Yvon-Durocher *et al* 2014, Rasilo *et al* 2015, Aben *et al* 2017, Sepulveda-Jauregui *et al* 2018). Therefore, the current rising temperatures can particularly intensify $CH_4$ emissions (Marotta *et al* 2014, Rasilo *et al* 2015, Aben *et al* 2017) due to changes both in $CH_4$ solubility and in the methanogenesis versus methanotrophy balance. On the other hand, the eutrophic reservoirs emit at least one order of magnitude more $CH_4$ than the oligotrophic ones. Indeed $CH_4$ emissions seem to be closely linked to primary productivity (Schmidt and Conrad 1993, Grossart *et al* 2011, Bogard *et al* 2014, Tang *et al* 2014, Deemer *et al* 2016). Phytoplankton-derived organic carbon appears to fuel higher rates of methane production than terrestrial-derived organic carbon (West *et al* 2012, 2016). Reservoir eutrophication is increasing worldwide as a result of the intensification of agriculture and the use of fertilizers (Canfield *et al* 2010, Heathcote and Downing 2012). Then, the expected increase in global temperatures along with reservoirs eutrophication might exacerbate $CH_4$ emissions.

The anthropogenic production of nitrogen fertilizer has doubled the inputs of this element to the Earth's surface, changing the nitrogen cycle. This change likely exceeds all the other human interventions in the cycles of nature (Gruber and Galloway 2008, Schlesinger 2009), but in comparison with the carbon cycle has received less attention (Battye *et al* 2017). Changes in land-use from forestal to agricultural or urban can boost the production of $N_2O$ due to nitrogen loadings into the aquatic systems (Seitzinger *et al* 2000, Mulholland *et al* 2008, Beaulieu *et al* 2011). $N_2O$ is produced aerobically by nitrification and anaerobically by denitrification depending on oxygen availability (Canfield *et al* 2010). In reservoirs, the few available data suggest that they are relevant in agricultural landscapes (Beaulieu *et al* 2015). Unfortunately, the importance of the reservoirs in global $N_2O$ emissions is practically unknown. Deemer *et al* (2016) estimated, using a very scarce database, that the global $N_2O$ emission from reservoirs is 0.03 Tg N $yr^{-1}$

accounting for 4% of the radiative forcing in a 100 year timescale.

Fluxes of $CO_2$, $CH_4$, and $N_2O$ have been reported mostly for tropical and boreal reservoirs, lacking the data of these fluxes in the Mediterranean biome, where the reservoirs are the preponderant aquatic ecosystems (Naselli-Flores 2003, Barros *et al* 2011, Lehner *et al* 2011, Morales-Pineda *et al* 2014, Deemer *et al* 2016). In this region, reservoirs provide drinking and irrigation water (Naselli-Flores 2003, Morales-Pineda *et al* 2014); consequently, they are close to agriculture and urban areas having high human pressure. Therefore, we need more simultaneous measurements of $CO_2$, $CH_4$, and $N_2O$ emissions in Mediterranean reservoirs submitted to contrasting anthropogenic pressure to get more accurate estimates of the global reservoir radiative forcing.

Here, we simultaneously measured the fluxes of $CO_2$, $CH_4$, and $N_2O$ in a group of Mediterranean reservoirs. We covered the vast idiosyncrasy of temperate reservoirs to obtain their radiative forcings in terms of $CO_2$ equivalents. We hypothesized that reservoirs located in anthropogenic landscapes would have higher radiative forcings than forestal reservoirs. Besides, we postulated that $CH_4$ emissions would be the main responsible for the positive radiative forcings.

## Methods

### Study reservoirs

We sampled 12 reservoirs between July 2016 and August 2017 in the South of Spain (figures 1(a), (b)). The reservoirs are located in watersheds with diverse lithology (figures 1(c), (d); supplementary figures 1–12 is available online at stacks.iop.org/ERL/15/044012/mmedia), different land-use (figures 1(e), (f); supplementary figures 13–24), morphometries, and ages (supplementary table 1). We quantified the $CO_2$, $CH_4$, and $N_2O$ fluxes using a PICARRO Cavity Ring-Down Spectroscopy (CRDS) gas analyzer connected to a floating chamber during the stratification (summer) and mixing (fall-winter) periods at one representative location. The reservoirs were built between 1932 and 2003, and they also differ in chemical and trophic characteristics with a range of chlorophyll-a from 0.6 to 18.6 $\mu$g $l^{-1}$ and a range of dissolved organic carbon (DOC) from 0.79 to 4.95 mg $l^{-1}$. More basic details on the study reservoirs in León-Palmero *et al* (2019) and supplementary tables 1 and 4. We collected data on reservoir area, capacity, age, watershed lithology, and land use from open databases (more details in supplementary methods).

### Quantification of $CO_2$, $CH_4$ and $N_2O$ fluxes

We measured $CO_2$, $CH_4$, and $N_2O$ fluxes using a high-resolution laser-based CRDS (PICARRO G2508) coupled to a floating chamber. For each reservoir in
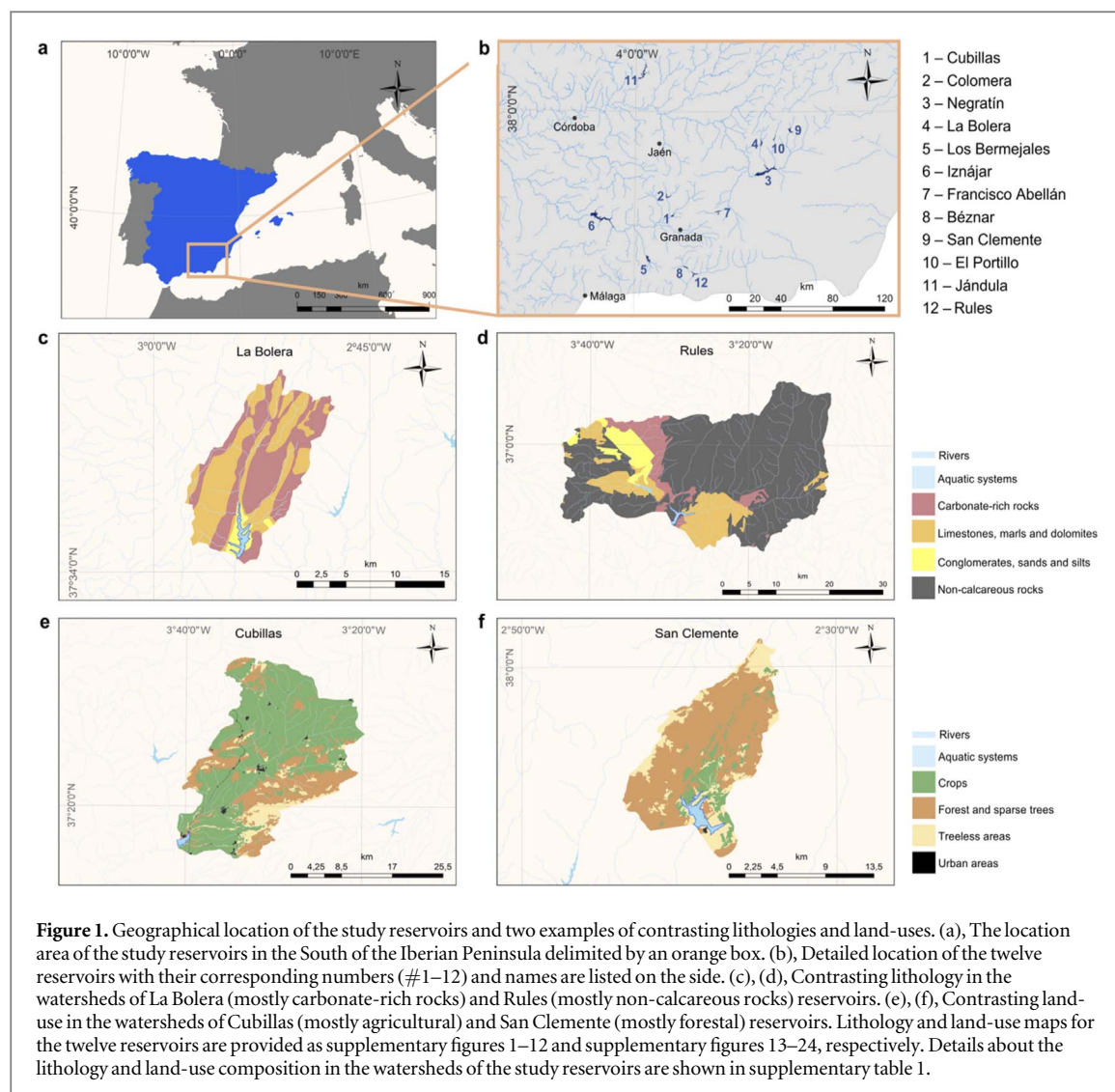
**Figure 1.** Geographical location of the study reservoirs and two examples of contrasting lithologies and land-uses. (a), The location area of the study reservoirs in the South of the Iberian Peninsula delimited by an orange box. (b), Detailed location of the twelve reservoirs with their corresponding numbers (#1–12) and names are listed on the side. (c), (d), Contrasting lithology in the watersheds of La Bolera (mostly carbonate-rich rocks) and Rules (mostly non-calcareous rocks) reservoirs. (e), (f), Contrasting land-use in the watersheds of Cubillas (mostly agricultural) and San Clemente (mostly forestal) reservoirs. Lithology and land-use maps for the twelve reservoirs are provided as supplementary figures 1–12 and supplementary figures 13–24, respectively. Details about the lithology and land-use composition in the watersheds of the study reservoirs are shown in supplementary table 1.

each sampling period, we took 3–5 measurements for 40 min. We calculated the daily (from 10 am to 4 pm) average and the standard error from these measurements. We obtained the flux calculation using the equation (1) (Zhao *et al* 2015):

$$Flux_{water-air} = \frac{b \cdot V \cdot P_0}{A \cdot R \cdot T_0}, \quad (1)$$

where $Flux_{water-air}$ ($\mu$mol m$^{-2}$ s$^{-1}$) is the flux from the water surface to the atmosphere; the $b$ (ppmv s$^{-1}$) value is the slope of the linear regression between the time and the concentration of each gas inside the chamber; the $V$ (m$^3$) is the floating chamber volume; the $A$ (m$^2$) is the floating chamber area; the $P_0$ (Pa) is the barometric pressure; the $R$ is the gas constant (8.314 m$^3$ Pa K$^{-1}$ mol$^{-1}$); and $T_0$ (K) is the ambient temperature. We checked that the slope was significantly different from zero for each measurement using a two-tailed t-Student test. We also calculated the coefficient of determination ($R^2$) for each measurement, accepting those whose $R^2 > 0.85$ (Moseman-Valtierra *et al* 2016). We measured ambient temperature, barometric pressure (HANNA HI 9828), and

wind speed (MASTECH MS6252A) at the beginning of each flux measurement.

Determination coefficients ($R^2$) for $CO_2$ fluxes were always >0.85. For $CH_4$ fluxes, most cases $R^2$ were >0.85, but it decreased until 0.65 when ebullition events were relevant. In these cases, we computed the $b$ value using the end-point concentrations and the time interval between them (equation (2)) (Zhao *et al* 2015):

$$b = \frac{[ppm\ CH_4]_f - [ppm\ CH_4]_i}{t_f - t_i}, \quad (2)$$

where $[ppmCH4]_f$ and $[ppmCH4]_i$ are the $CH_4$ concentration in the floating chamber at the end and the beginning of the time considered; $t_f$ and $t_i$ are the time at the end and the beginning of the measurement.

For $N_2O$ flux measurements, most of $R^2$ values were low (even when the regression was significantly different from zero). For those cases, we first checked the analyzer precision (<25 ppb). If the changes were larger than the analyzer precision, we assumed these fluxes were different from zero. We also compared the $N_2O$ fluxes with the percentage of saturation of dissolved $N_2O$ in the water column. Details for the

measurements of dissolved $N_2O$ are in supplementary methods. $N_2O$ undersaturated waters and negative slopes mean $N_2O$ influxes (i.e. $N_2O$ sinks). By contrast, $N_2O$ supersaturated waters and positive slopes mean $N_2O$ outfluxes (i.e. $N_2O$ sources).

To obtain the reservoir radiative forcings we summed the corresponding forcing due to $CO_2$ emissions, the warming potential (GWP) of $CH_4$ in terms of $CO_2$ equivalents, and the warming potential of $N_2O$ in terms of $CO_2$ equivalents. We used 34 to convert $CH_4$ in $CO_2$ equivalent and 298 to convert $N_2O$ in $CO_2$ equivalent in a 100 year time horizon, including the climate-carbon feedbacks (IPCC 2013).

### C, N and P analysis in the water column

We sampled the epilimnion of each reservoir for C, N and, P analysis. We measured total nutrient concentrations using unfiltered water, while we filtered through 0.7 $\mu$m pore-size Whatman GF/F glass-fiber filters samples for dissolved nutrients. We acidified with phosphoric acid (final pH $< 2$) the samples for DOC, total dissolved nitrogen (TDN), and total nitrogen (TN). We measured DOC, dissolved inorganic carbon (DIC), TN, and TDN by high–temperature catalytic oxidation using a Shimadzu total organic carbon (TOC) analyzer (Model TOC-V CSH) coupled to nitrogen analyzer (TNM-1) (Álvarez-Salgado and Miller 1998). The instrument was calibrated using a four-point standard curve of dried potassium hydrogen phthalate for DOC, dried sodium bicarbonate and sodium carbonate for DIC, and dried potassium nitrate for TN and TDN. We analyzed two replicates and three to five injections per replicate for each sample. Samples for DOC analysis were purged with phosphoric acid for 20 min to eliminate DIC.

We measured the $NO_3^-$ concentration using the ultraviolet spectrophotometric method, using a Perkin Elmer UV-Lambda 40 spectrophotometer at wavelengths of 220 nm and correcting for DOC absorbance at 275 nm (Baird *et al* 2012). We measured $NH_4^+$ and $NO_2^-$ concentrations by inductively coupled plasma optical emission spectrometry. Total phosphorus concentration was measured by triplicate using the molybdenum blue method (Murphy and Riley 1962) after digestion with a mixture of potassium persulphate and boric acid at 120 °C for 30 min (Baird *et al* 2012).

We also measured dissolved $CH_4$ and $N_2O$ by headspace equilibration in a 50 ml air-tight glass syringe by duplicate in the water column (Sierra *et al* 2017a, 2017b). We analyzed simultaneously the concentration of dissolved $CH_4$ and $N_2O$ using gas chromatography (more details in supplementary methods).

### Biological analyses and reservoir metabolism

We determined chlorophyll-*a* concentration by collecting the particulate material of 500 to 2000 ml of water by filtering through 0.7 $\mu$m pore-size Whatman GF/F glass-fiber filters, then extracting the filters with 95% methanol in the dark at 4 °C for 24 h (Baird *et al* 2012). We measured pigment absorption using a Perkin Elmer UV-Lambda 40 spectrophotometer at wavelengths of 665 and 750 nm for scattering correction.

We recorded dissolved oxygen concentration and temperature using a miniDOT (PME) submersible water logger during the stratification period. We got measurements every 10 min for 24–48 h. We established the start and ended time for photosynthesis as 30 min before sunrise and 30 min after dawn (Schlesinger and Bernhardt 2013). We calculated the respiration rate during the night (the period between 60 min after dawn and 60 min before sunrise) (Staehr *et al* 2010), and we assumed that the respiration rate overnight was similar to the respiration rate over the day. The equations used to calculate lake metabolism were taken from Staehr *et al* (2010).
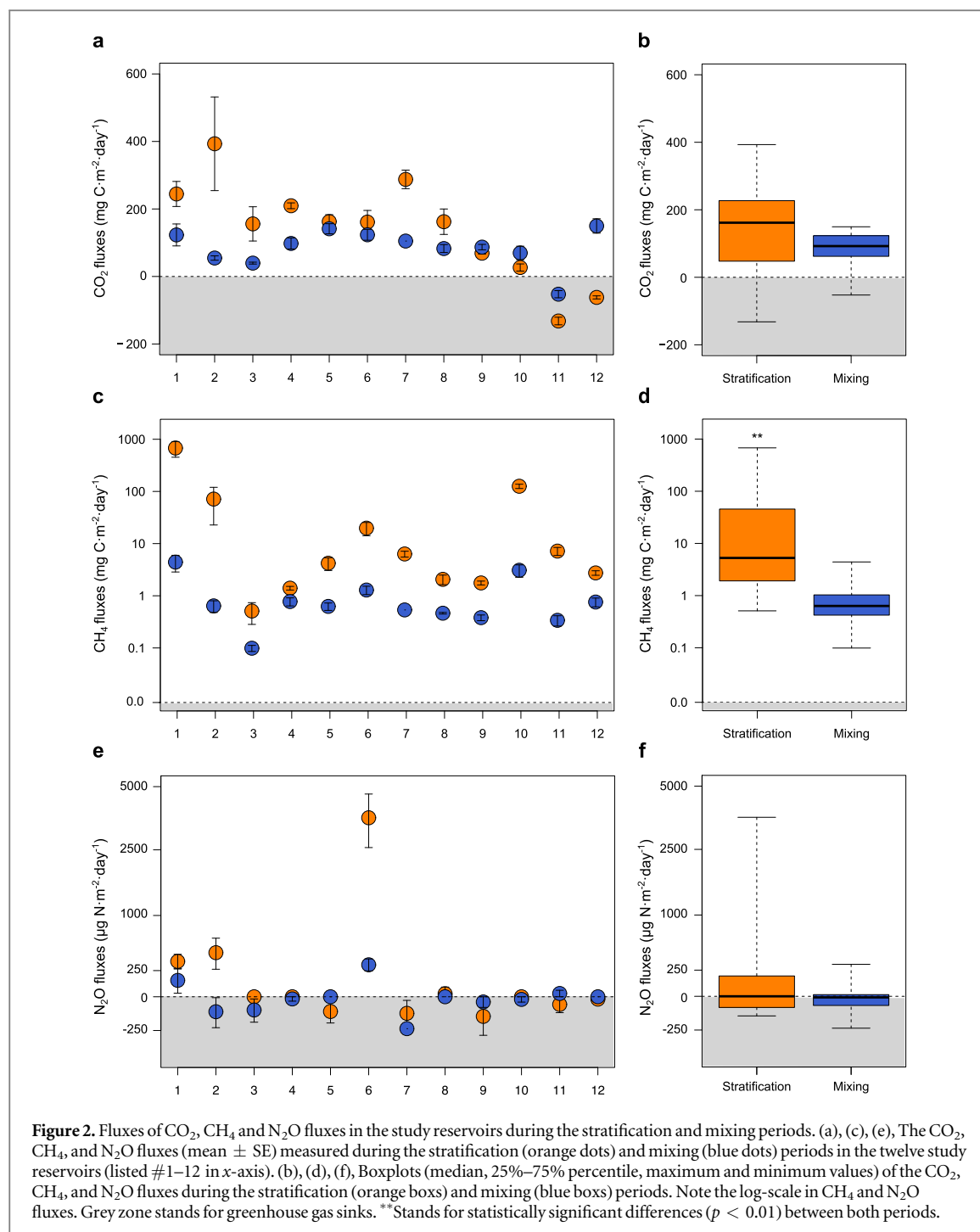
### Statistical tests

We performed all the statistical analysis in R (R Core Team 2014) using the packages car (Fox and Weisberg 2011), nortest (Gross and Ligges 2015), and mgcv (Wood 2011). More details on T-test and generalized additive models (GAMs) (Wood 2006) in supplementary methods.

## Results and discussion

### $CO_2$, $CH_4$ and $N_2O$ fluxes

We found that some reservoirs were sinks (fluxes $< 0$) and other sources (fluxes $> 0$) for $CO_2$ and $N_2O$ fluxes, but all reservoirs were $CH_4$ sources (figure 2, supplementary table 2). The daily average of $CO_2$ fluxes ranged from $-131.97$ to $393.11$ mg C m$^{-2}$ d$^{-1}$ during the stratification period (figure 2(a), orange dots) and from $-52.51$ to $149.62$ mg C m$^{-2}$ d$^{-1}$ during the mixing period (figure 2(a), blue dots). We measured the lower value in the Jándula reservoir (#11) consistently in both periods. We did not find significant differences between the stratification and mixing periods (figure 2(b); supplementary table 3). The median of these fluxes in both periods was $114.00$ mg C m$^{-2}$ d$^{-1}$, similar to previous data for northern temperate reservoirs (Barros *et al* 2011) and smaller than the fluxes measured in other Mediterranean reservoirs (Morales-Pineda *et al* 2014, Samiotis *et al* 2018), and the global average estimated by Deemer *et al* (2016).

The daily average of $CH_4$ fluxes varied more than three orders of magnitude from $0.51$ to $678.84$ mg C m$^{-2}$ d$^{-1}$ during the stratification period (figure 2(c), orange dots) and from $0.10$ to $4.41$ mg C m$^{-2}$ d$^{-1}$ during the mixing period (figure 2(c), blue dots). The maximum values were reached in Cubillas (#1), a shallow reservoir with evident ebullition fluxes. The

**Figure 2.** Fluxes of $CO_2$, $CH_4$ and $N_2O$ fluxes in the study reservoirs during the stratification and mixing periods. (a), (c), (e), The $CO_2$, $CH_4$, and $N_2O$ fluxes (mean $\pm$ SE) measured during the stratification (orange dots) and mixing (blue dots) periods in the twelve study reservoirs (listed #1–12 in $x$-axis). (b), (d), (f), Boxplots (median, 25%–75% percentile, maximum and minimum values) of the $CO_2$, $CH_4$, and $N_2O$ fluxes during the stratification (orange boxes) and mixing (blue boxes) periods. Note the log-scale in $CH_4$ and $N_2O$ fluxes. Grey zone stands for greenhouse gas sinks. **Stands for statistically significant differences ($p < 0.01$) between both periods.

median value during the stratification period was 5.27 mg C m$^{-2}$ d$^{-1}$, whereas during the mixing period was 0.63 mg C m$^{-2}$ d$^{-1}$. Emissions were significantly higher during the summer stratification than during the winter mixing (figure 2(d); supplementary table 3) as it has been found in previous works (Beaulieu *et al* 2014, Musenze *et al* 2014) and emphasized the need to perform seasonal studies to obtain accurate annual rates of $CH_4$ emissions. This wide range in $CH_4$ emissions covers from typical values found in tropical reservoirs to values found in northern temperate reservoirs (Barros *et al* 2011), although lower than in other Mediterranean reservoirs (Samiotis *et al* 2018).

The daily average of $N_2O$ fluxes ranged from −154.03 to 3600.88 μgN m$^{-2}$ d$^{-1}$ during the stratification period (figure 2(e), orange dots) and from −238.08 to 313.44 μgN m$^{-2}$ d$^{-1}$ during the mixing period (figure 2(e), blue dots). In both periods, we obtained the maximum values in the Iznájar reservoir (#6). We did not find significant differences between stratification and mixing periods (figure 2(f); supplementary table 3). The median value was 0.00 μgN m$^{-2}$ d$^{-1}$ acting globally as neutral systems. In the particular case of the Iznájar reservoir (#6), however, it acted as a relevant source of $N_2O$ with values similar to those found in tropical reservoirs (Guérin *et al* 2006). $N_2O$

flux variability in these Mediterranean reservoirs was more comprehensive than the variability found in boreal lakes and reservoirs (Soued *et al* 2015).

### CO$_2$ flux drivers

To determine the main drivers (predictors) of GHG fluxes in the study reservoirs, we used GAMs (see supplementary methods, supplementary tables 4 and 5). The inputs of dissolved inorganic and organic carbon and net ecosystem metabolism (i.e. the budget between photosynthesis and respiration) are considered the main drivers of CO$_2$ fluxes in lakes and reservoir (Tranvik *et al* 2009, McDonald *et al* 2013, Marcé *et al* 2015, Weyhenmeyer *et al* 2015). In fact, the non-calcareous area in the watershed and the reservoir respiration were the main drivers of CO$_2$ fluxes during the stratification period with a fit deviance of 93.4% (Log$_{10}$ (CO$_2$ + 150) = −6.6 10$^{-4}$ non-calcareous area + 1.70 log$_{10}$ (Respiration rate)$^{0.35}$) and an explained variance of 91% (figure 3(a); supplementary table 5). The non-calcareous area in the watershed was a linear function inversely related to CO$_2$ fluxes (figure 3(b)), and most of the deviance was 90.7%, whereas respiration only explained the 9.4%. Unlike this linear function, reservoir respiration showed a power function with the CO$_2$ flux (figure 3(c)). The smaller the calcareous watershed, the lower the export of DIC is. Indeed, we found a significant and negative relationship between non-calcareous area and the DIC concentration in the reservoirs irrespectively of the sampling period (linear regression results $n = 24$, $R^2 = 0.50$, $p < 0.001$) (figure 3(d)). This result agrees with previous studies showing that a significant fraction of CO$_2$ emissions in boreal lakes is related to inorganic carbon loading from watershed (Weyhenmeyer *et al* 2015). In other Mediterranean reservoirs, carbonate weathering was also related to CO$_2$ supersaturation and, consequently, to CO$_2$ evasion (López *et al* 2011, Marcé *et al* 2015). We obtained a significant and positive function between reservoir respiration and the concentration of chlorophyll-a during the stratification period (linear regression results $n = 12$, $R^2 = 0.43$, $p < 0.05$) (figure 3(e)), but not with the concentration of DOC (linear regression results $n = 12$, $p = 0.64$). Overall, we show, for the first time, a remarkable and direct link between watershed lithology and the CO$_2$ fluxes from reservoirs.
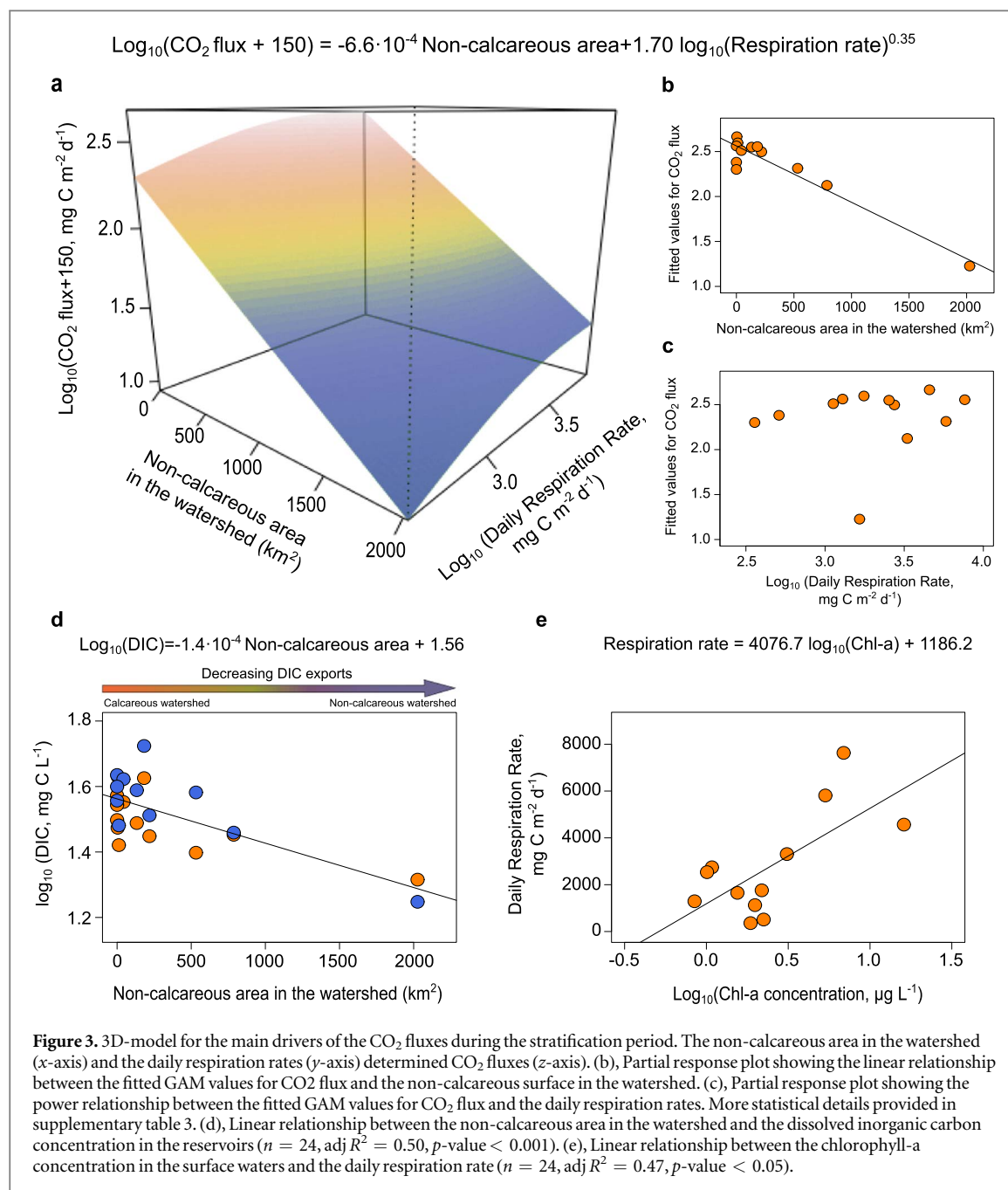
### CH$_4$ flux drivers

CH$_4$ emissions from a reservoir depend on its net production (i.e. the budget between methanogenesis and methanotrophy) and its storage capacity into the water column. Dissolved CH$_4$ storage is related to water mean depth (i.e. the higher the hydrostatic pressure, the higher storage capacity is) and temperature (i.e. the lower temperature, the higher solubility is) (Keller and Stallard 1994, West *et al* 2016).

Shallow systems are prone to have warmer waters, higher sediment exposure enhancing significantly CH$_4$ ebullition rates, and, consequently, less capacity to store CH$_4$ (Keller and Stallard 1994, Marotta *et al* 2014, Aben *et al* 2017). In the study reservoirs, we obtained that water temperature and reservoir mean depth were the main drivers of the CH$_4$ emissions with a fit deviance of 65.0% and an explained variance of 59% (Log$_{10}$ (CH$_4$ flux + 1) = 6.6 10$^{-2}$ Temperature −0.82 + 2.5 10$^{-4}$ e$^{(8.44/\log_{10}(\text{mean depth}))}$) (figure 4(a); supplementary table 3). CH$_4$ emission rate was a linear and positive function of water temperature (figure 4(b)) and accounted for 38.1% of the fit deviance. CH$_4$ emission rate resulted in a negative exponential function of the reservoir mean depth (figure 4(c)) with fit deviance of 27.6%. At mean depths shallower than 16 meters, the CH$_4$ emissions increased exponentially (i.e. 1.2 in figure 4(c)). CH$_4$ emissions depended on concentration of CH$_4$ in the surface waters following a power function (figure 4(d)) ($n = 24$, $R^2 = 0.87$, $p < 0.001$). Previous studies have shown that CH$_4$ concentration in the water column is related to chlorophyll-a concentration (Schmidt and Conrad 1993, Grossart *et al* 2011, Bogard *et al* 2014, Tang *et al* 2014). We also found a positive and linear relationship between the concentration of chlorophyll-a and the concentration of CH$_4$ in the surface waters ($n = 24$, $R^2 = 0.19$, $p < 0.05$) (figure 4(e)), but not directly with the emissions. Recent studies point out the eutrophication as the primary driver of CH$_4$ emissions (Deemer *et al* 2016, Beaulieu *et al* 2019).

### N$_2$O flux drivers

Nitrogen loading derived from human activities affects N$_2$O emissions from inland waters (Seitzinger *et al* 2000, Mulholland *et al* 2008, Baulch *et al* 2011, Beaulieu *et al* 2011). It is widely acknowledged that the N$_2$O production increases in streams and reservoirs located in agricultural and urban landscapes as a consequence of nitrate loading (Mulholland *et al* 2008, Baulch *et al* 2011, Beaulieu *et al* 2011, 2015). In the study reservoirs, consistently, the GAMs result showed that the TN concentration was the main driver of N$_2$O fluxes along with the wind speed (Log$_{10}$ (N$_2$O flux + 240) = 0.72 e$^{0.21 \text{ TN}}$ + 1.30 Wind speed$^{0.21}$) with a fit deviance of 82.7% and an explained variance of 79.8% (figure 5(a); supplementary table 5). N$_2$O fluxes were an exponential function of TN concentration and explained most of the deviance 52.2% (figure 5(b)). Wind speed showed a positive power function with the fluxes and only explained 13.9% (figure 5(c)).
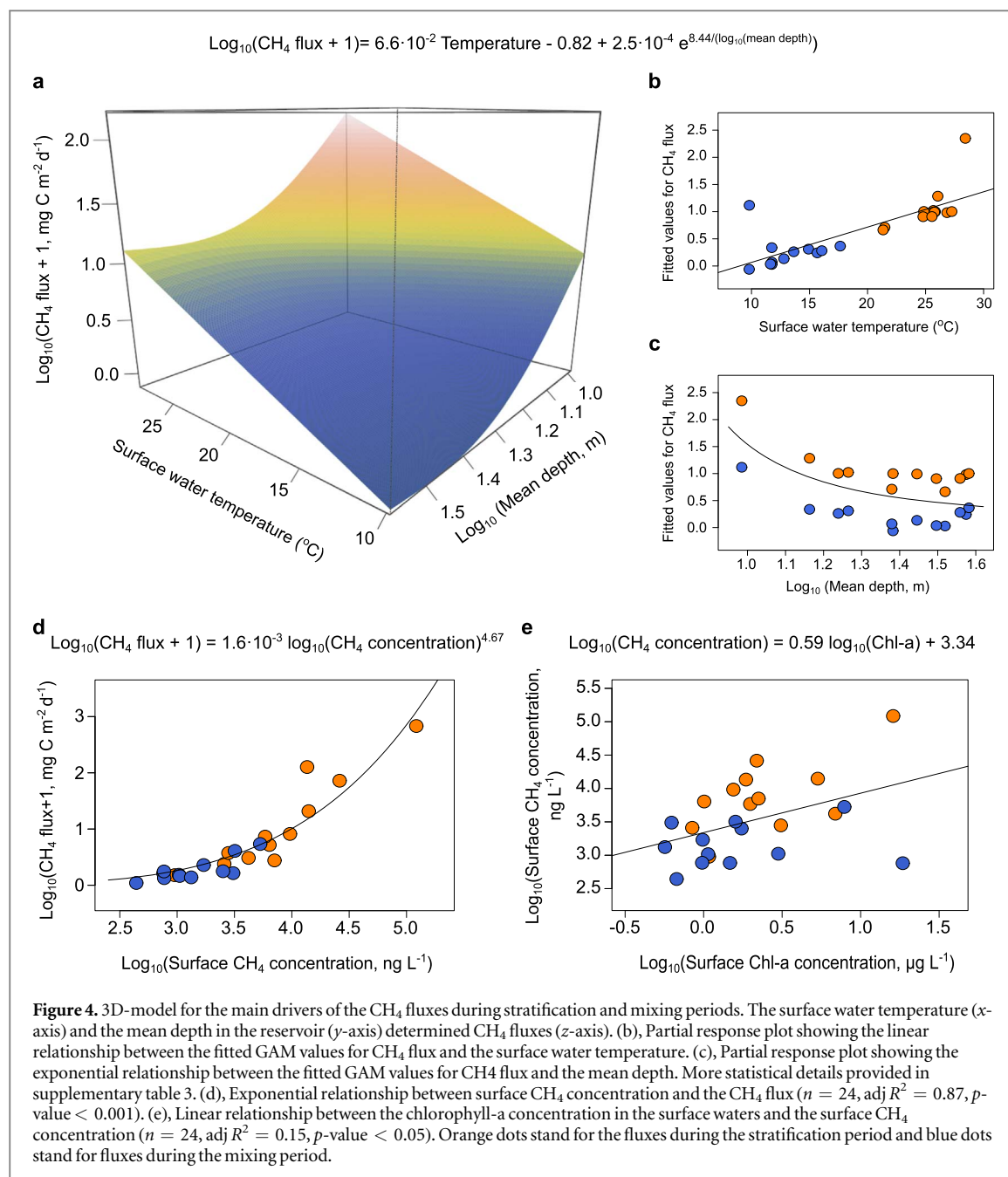
We determined the anthropogenic pressure in the reservoir watershed as the ratio of the area with crops plus the urban area divided by the forest area (i.e. the anthropogenic land-use ratio). We found a significant and positive relationship between this land-use ratio

**Figure 3.** 3D-model for the main drivers of the $CO_2$ fluxes during the stratification period. The non-calcareous area in the watershed (*x*-axis) and the daily respiration rates (*y*-axis) determined $CO_2$ fluxes (*z*-axis). (b), Partial response plot showing the linear relationship between the fitted GAM values for CO2 flux and the non-calcareous surface in the watershed. (c), Partial response plot showing the power relationship between the fitted GAM values for $CO_2$ flux and the daily respiration rates. More statistical details provided in supplementary table 3. (d), Linear relationship between the non-calcareous area in the watershed and the dissolved inorganic carbon concentration in the reservoirs ($n = 24$, adj $R^2 = 0.50$, *p*-value < 0.001). (e), Linear relationship between the chlorophyll-a concentration in the surface waters and the daily respiration rate ($n = 24$, adj $R^2 = 0.47$, *p*-value < 0.05).

and the concentration of TN in the reservoir waters ($n = 24$, $R^2 = 0.60$, $p < 0.001$) (figure 5(d); supplementary table 6). Both crops and urban areas increased the nitrogen concentration in their different compounds (TN, TDN, $NO_3^-$ and $NO_2^-$) (supplementary table 6). The urban area, in square kilometer or in its percentage relative in the watershed, showed a higher slope than the slope in the crop areas (figure 5(e)). Therefore, the impact of urban development on nitrogen inputs is even higher than the influence of crop areas.

$N_2O$ fluxes were a nonlinear function of the anthropogenic land-use ratio (figure 5(f)). For anthropogenic land-use ratios higher than 1 (i.e. crops and urban areas predominance over the forest area), the $N_2O$ fluxes increased exponentially

(figure 5(f)). In contrast, we observed that for watersheds with forestal coverage more extensive than ∼40% of watershed, the $N_2O$ emissions decreased drastically, even becoming an $N_2O$ sink (figure 5(g)). Other authors also found than boreal forest reservoirs acted as $N_2O$ sinks (Hendzel *et al* 2005). Therefore, the relevance of the nitrogen inputs from watershed on $N_2O$ fluxes is mostly dependent on the anthropogenic land-use. Our results suggest an exponential influence of the agricultural and, mainly, urban areas in the watershed on the $N_2O$ emissions. However, most of the previous studies have been mainly focused on the agricultural effects (Baulch *et al* 2011, Musenze *et al* 2014, Beaulieu *et al* 2015), relegating the urban influence on the background.

**Figure 4.** 3D-model for the main drivers of the $CH_4$ fluxes during stratification and mixing periods. The surface water temperature (*x*-axis) and the mean depth in the reservoir (*y*-axis) determined $CH_4$ fluxes (*z*-axis). (b), Partial response plot showing the linear relationship between the fitted GAM values for $CH_4$ flux and the surface water temperature. (c), Partial response plot showing the exponential relationship between the fitted GAM values for CH4 flux and the mean depth. More statistical details provided in supplementary table 3. (d), Exponential relationship between surface $CH_4$ concentration and the $CH_4$ flux ($n = 24$, adj $R^2 = 0.87$, *p*-value $< 0.001$). (e), Linear relationship between the chlorophyll-a concentration in the surface waters and the surface $CH_4$ concentration ($n = 24$, adj $R^2 = 0.15$, *p*-value $< 0.05$). Orange dots stand for the fluxes during the stratification period and blue dots stand for fluxes during the mixing period.

## Reservoir radiative forcings in $CO_2$ equivalents

We obtained a variability range in the GHG fluxes larger than the latitudinal variability reported in previous works (Barros *et al* 2011). The radiative forcings due to the GHG emissions from the reservoirs differed substantially between the stratification (summer) and the mixing (fall-winter) (figure 6). Radiative forcings were substantially higher during the stratification than during the mixing. This difference could be related to the significantly higher emissions of $CH_4$ during the stratification than mixing (figure 2). Methanogenesis is a microbial process particularly sensitive to temperature (Marotta *et al* 2014, Yvon-Durocher *et al* 2014, Rasilo *et al* 2015, Aben *et al* 2017, Sepulveda-Jauregui *et al* 2018) that increase during summer. In addition, water mean depth decrease during this season and

these factors also affect to the $CH_4$ emissions (figure 4). Radiative forcings ranged from 124.53 mg $CO_2$ equivalents m$^{-2}$ d$^{-1}$ in Rules reservoir (#12) to 31,884.03 mg $CO_2$ equivalents m$^{-2}$ d$^{-1}$ in Cubillas reservoir (#1) (supplementary table 2). These last values were even higher than those found for tropical plantations (Laine *et al* 2016). In stratification, $CH_4$ emissions contributed significantly to the total radiative forcing (in terms of $CO_2$ equivalent), ranging from 3.9% to 98.32% (figure 6(a) purple sector). In contrast, the $CO_2$ emissions contributed to the total radiative forcing mostly during the mixing (fall and winter), accounting for up to 97% (figure 6(b) blue sector). During the mixing, the radiative forcing ranged from 28.68 mg $CO_2$ equivalents m$^{-2}$ d$^{-1}$ in Jándula reservoir (#11) to 721.65 mg $CO_2$ equivalents m$^{-2}$ d$^{-1}$ in Cubillas
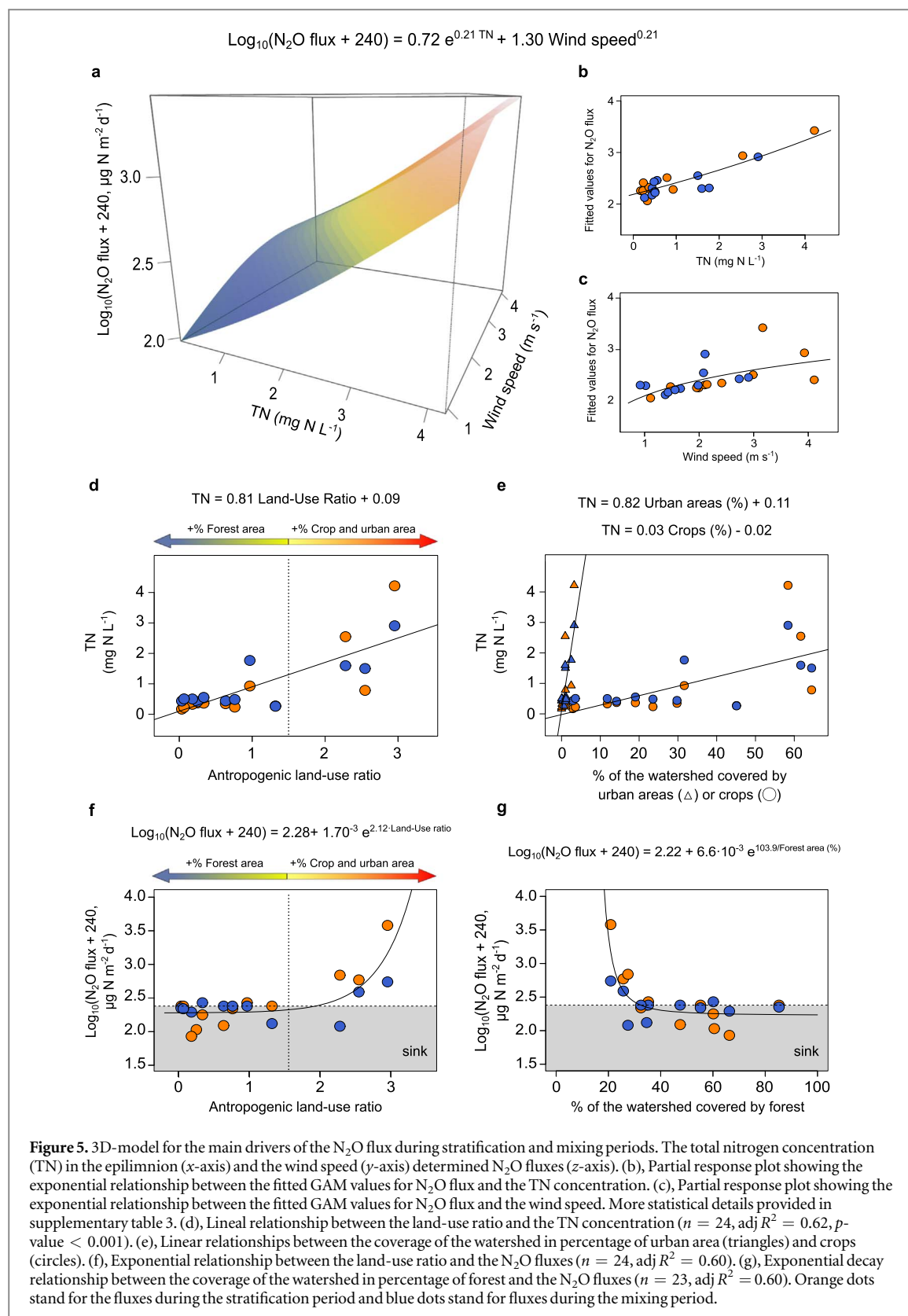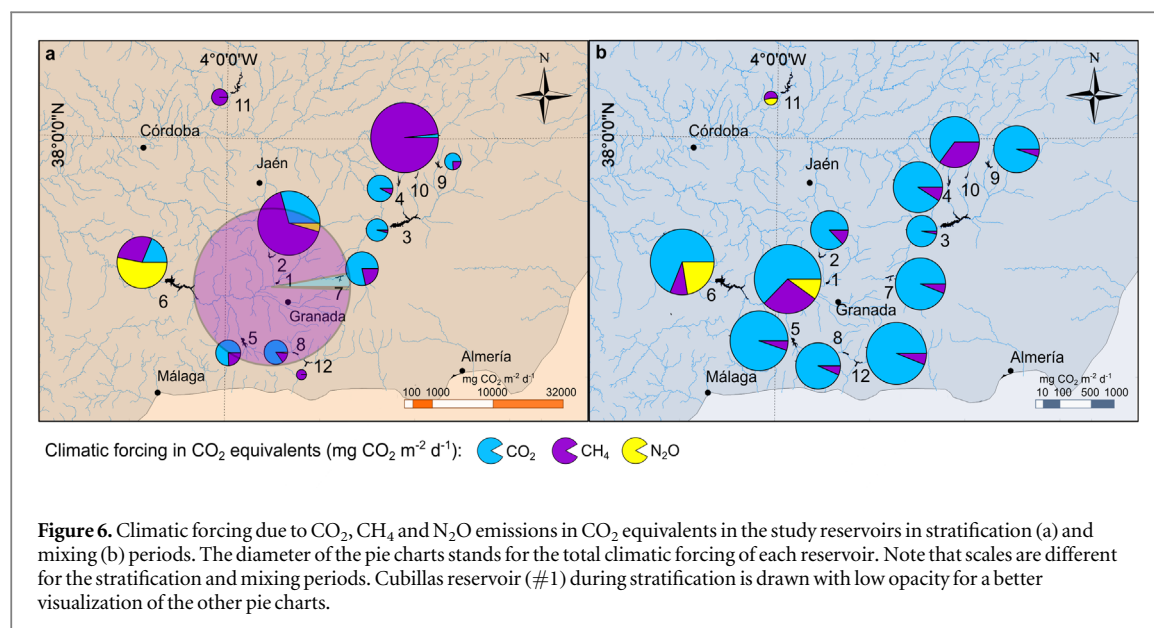
**Figure 5.** 3D-model for the main drivers of the N₂O flux during stratification and mixing periods. The total nitrogen concentration (TN) in the epilimnion ($x$-axis) and the wind speed ($y$-axis) determined N₂O fluxes ($z$-axis). (b), Partial response plot showing the exponential relationship between the fitted GAM values for N₂O flux and the TN concentration. (c), Partial response plot showing the exponential relationship between the fitted GAM values for N₂O flux and the wind speed. More statistical details provided in supplementary table 3. (d), Lineal relationship between the land-use ratio and the TN concentration ($n = 24$, adj $R^2 = 0.62$, $p$-value $< 0.001$). (e), Linear relationships between the coverage of the watershed in percentage of urban area (triangles) and crops (circles). (f), Exponential relationship between the land-use ratio and the N₂O fluxes ($n = 24$, adj $R^2 = 0.60$). (g), Exponential decay relationship between the coverage of the watershed in percentage of forest and the N₂O fluxes ($n = 23$, adj $R^2 = 0.60$). Orange dots stand for the fluxes during the stratification period and blue dots stand for fluxes during the mixing period.

reservoir (#1) (supplementary table 2). The contribution of N₂O emissions to the radiative forcing in the study reservoirs was secondary (supplementary table 2) with the exception of the Iznájar reservoir (#6) in both periods (figure 6) and the Cubillas and Jándula reservoirs (#1 and 11) during the mixing (figure 6(b)). In the Iznájar reservoir, the N₂O

emissions accounted for up to 53.1% of the radiative forcing during the stratification, whereas during the mixing period was 22.32% (supplementary table 2). CO₂ and N₂O emissions were driven by external factors as lithology and land-use without significant differences between mixing and stratification. In contrast, CH₄ emissions were driven by internal

**Figure 6.** Climatic forcing due to $CO_2$, $CH_4$ and $N_2O$ emissions in $CO_2$ equivalents in the study reservoirs in stratification (a) and mixing (b) periods. The diameter of the pie charts stands for the total climatic forcing of each reservoir. Note that scales are different for the stratification and mixing periods. Cubillas reservoir (#1) during stratification is drawn with low opacity for a better visualization of the other pie charts.

factors as water temperature and mean depth with higher emissions during stratification, which affected the total radiative forcings of the reservoirs.

Future climatic scenarios for the Mediterranean biome suggest substantial warming, a decrease in total precipitation, and extreme heat-waves and heavy precipitations (Giorgi and Lionello 2008) that likely will enhance the $CH_4$ emissions due to a reduction in reservoir depth (i.e. lower precipitation and higher evaporation) and an increase in the water temperatures. Climatic change may also affect nutrient loading by runoff to the reservoirs. Hydrological models for Mediterranean watersheds suggest that nutrient concentrations in reservoirs may increase despite a runoff reduction (Molina-Navarro *et al* 2014). The potential increase in the N and P concentrations will boost water eutrophication and the resulting emissions of $N_2O$ (Mulholland *et al* 2008, Baulch *et al* 2011, Beaulieu *et al* 2015) and $CH_4$ (Deemer *et al* 2016, Beaulieu *et al* 2019). Temperature increases and eutrophication may also have synergic effects on $CH_4$ emissions (Davidson *et al* 2018, Sepulveda-Jauregui *et al* 2018). Policies to reduce the fertilizers used in agricultural areas and, in particular, to promote the tertiary wastewater treatment in urban areas may decrease N and P loading to prevent water resources degradation and reduce GHG emissions and their subsequent radiative forcings from the already constructed reservoirs. For the construction of the projected reservoirs, the selection of optimal locations should consider that siliceous bedrock, in forestal locations, and deep canyons can minimize or even offset the GHG emissions and, consequently, reduce their radiative forcings.

## Data availability statement

The data that support the findings of this study are included within the article in supplementary material.

## ORCID iDs

Elizabeth León-Palmero ⬤ https://orcid.org/0000-0001-8220-1188
Rafael Morales-Baquero ⬤ https://orcid.org/0000-0002-7075-7899
Isabel Reche ⬤ https://orcid.org/0000-0003-2908-1724

## References

Aben R C H *et al* 2017 Cross continental increase in methane ebullition under climate change *Nat. Commun.* **8** 1682

Álvarez-Salgado X A and Miller A E J 1998 Simultaneous determination of dissolved organic carbon and total dissolved nitrogen in seawater by high temperature catalytic oxidation: conditions for precise shipboard measurements *Mar. Chem.* **62** 325–33

Baird R B *et al* 2012 *Standard Methods for the Examination of Water and Wastewater* vol 10 ed E W Rice (Washington, DC: American Public Health Association)

Barros N, Cole J J, Tranvik L J, Prairie Y T, Bastviken D, Huszar V L M, del Giorgio P and Roland F 2011 Carbon emission from hydroelectric reservoirs linked to reservoir age and latitude *Nat. Geosci.* **4** 593–6

Bastviken D, Tranvik L J, Downing J A, Crill P M and Enrich-Prast A 2011 Freshwater methane emissions offset the continental carbon sink *Science* **331** 50–50

Battye W, Aneja V P and Schlesinger W H 2017 Is nitrogen the next carbon? *Earth's Future* **5** 894–904

Baulch H M, Schiff S L, Maranger R and Dillon P J 2011 Nitrogen enrichment and the emission of nitrous oxide from streams *Glob. Biogeochem. Cycles* **25** 15

Beaulieu J J, DelSontro T and Downing J A 2019 Eutrophication will increase methane emissions from lakes and impoundments during the 21st century *Nat. Commun.* **10** 1375

Beaulieu J J, Nietch C T and Young J L 2015 Controls on nitrous oxide production and consumption in reservoirs of the Ohio River Basin *J. Geophys. Res.—Biogeosci.* **120** 1995–2010

Beaulieu J J, Smolenski R L, Nietch C T, Townsend-Small A and Elovitz M S 2014 High methane emissions from a midlatitude reservoir draining an agricultural watershed *Environ. Sci. Technol.* **48** 11100–8

Beaulieu J J *et al* 2011 Nitrous oxide emission from denitrification in stream and river networks *PNAS* **108** 214–9

Bogard M J, del Giorgio P A, Boutet L, Chaves M C G, Prairie Y T, Merante A and Derry A M 2014 Oxic water column methanogenesis as a major component of aquatic $CH_4$ fluxes *Nat. Commun.* **5** 5350

Canfield D E, Glazer A N and Falkowski P G 2010 The evolution and future of earth's nitrogen cycle *Science* **330** 192–6

Cole J J, Caraco N F, Kling G W and Kratz T K 1994 Carbon dioxide supersaturation in the surface waters of lakes *Science* **265** 1568–70

Davidson T A, Audet J, Jeppesen E, Landkildehus F, Lauridsen T L, Søndergaard M and Syväranta J 2018 Synergy between nutrients and warming enhances methane ebullition from experimental lakes *Nat. Clim. Change* **8** 156–60

Deemer B R, Harrison J A, Li S, Beaulieu J J, DelSontro T, Barros N, Bezerra-Neto J F, Powers S M, dos Santos M A and Vonk J A 2016 Greenhouse gas emissions from reservoir water surfaces: a new global synthesis *BioScience* **66** 949–64

Fox J and Weisberg S 2011 *An R Companion to Applied Regression* (Thousand Oaks, CA: Sage)

Giorgi F and Lionello P 2008 Climate change projections for the Mediterranean region *Glob. Planet. Change* **63** 90–104

Gross J and Ligges U 2015 *nortest: Tests for Normality*(https://CRAN.R-project.org/package=nortest)

Grossart H-P, Frindte K, Dziallas C, Eckert W and Tang K W 2011 Microbial methane production in oxygenated water column of an oligotrophic lake *PNAS* **108** 19657–61

Gruber N and Galloway J N 2008 An Earth-system perspective of the global nitrogen cycle *Nature* **451** 293–6

Guérin F, Abril G, Richard S, Burban B, Reynouard C, Seyler P and Delmas R 2006 Methane and carbon dioxide emissions from tropical reservoirs: significance of downstream rivers *Geophys. Res. Lett.* **33** L21407

Heathcote A J and Downing J A 2012 Impacts of eutrophication on carbon burial in freshwater lakes in an intensively agricultural landscape *Ecosystems* **15** 60–70

Hendzel L L, Matthews C J D, Venkiteswaran J J St., Louis V L, Burton D, Joyce E M and Bodaly R A 2005 Nitrous oxide fluxes in three experimental boreal forest reservoirs *Environ. Sci. Technol.* **39** 4353–60

IPCC 2013 *Climate Change 2013: The Physical Science Basis. Contribution of Working Group I to the Fifth Assessment Report of the Intergovernmental Panel on Climate Change* ed T F Stocker *et al* (Cambridge: Cambridge University Press)

Keller M and Stallard R F 1994 Methane emission by bubbling from Gatun Lake, Panama *J. Geophys. Res.* **99** 8307–19

Laine J, Joosten H, Sirin A, Couwenberg J and Smith P 2016 The role of peatlands in climate regulation *Peatland Restoration and Ecosystem Services: Science, Policy and Practice* ed A Bonn *et al* (Cambridge: Cambridge University Press)

Lehner B *et al* 2011 High-resolution mapping of the world's reservoirs and dams for sustainable river-flow management *Front. Ecol. Environ.* **9** 494–502

León-Palmero E, Reche I and Morales-Baquero R 2019 Atenuación de luz en embalses del sur-este de la Península Ibérica *Ingeniería del agua* **23** 65–75

López P, Marcé R and Armengol J 2011 Net heterotrophy and $CO_2$ evasion from a productive calcareous reservoir: adding complexity to the metabolism-$CO_2$ evasion issue *J. Geophys. Res.* **116** G02021

Le Quéré C L *et al* 2018 Global carbon budget 2018 *Earth Syst. Sci. Data* **10** 2141–94

Marcé R, Obrador B, Morguí J-A, Riera J L, López P and Armengol J 2015 Carbonate weathering as a driver of $CO_2$ supersaturation in lakes *Nat. Geosci.* **8** 107–11

Marotta H, Pinho L, Gudasz C, Bastviken D, Tranvik L J and Enrich-Prast A 2014 Greenhouse gas production in low-latitude lake sediments responds strongly to warming *Nat. Clim. Change* **4** 467–70

McDonald C P, Stets E G, Striegl R G and Butman D 2013 Inorganic carbon loading as a primary driver of dissolved carbon dioxide concentrations in the lakes and reservoirs of the contiguous United States *Glob. Biogeochem. Cycles* **27** 285–95

Molina-Navarro E, Trolle D, Martínez-Pérez S, Sastre-Merlín A and Jeppesen E 2014 Hydrological and water quality impact assessment of a Mediterranean limno-reservoir under climate change and land use management scenarios *J. Hydrol.* **509** 354–66

Morales-Pineda M, Cózar A, Laiz I, Úbeda B and Gálvez J Á 2014 Daily, biweekly, and seasonal temporal scales of $pCO_2$ variability in two stratified Mediterranean reservoirs *J. Geophys. Res. Biogeosci.* **119** 2013JG002317

Moseman-Valtierra S *et al* 2016 Carbon dioxide fluxes reflect plant zonation and belowground biomass in a coastal Marsh *Ecosphere* **7** e01560

Mulholland P J *et al* 2008 Stream denitrification across biomes and its response to anthropogenic nitrate loading *Nature* **452** 202

Murphy J and Riley J P 1962 A modified single solution method for the determination of phosphate in natural waters *Anal. Chim. Acta* **27** 31–6

Musenze R S, Grinham A, Werner U, Gale D, Sturm K, Udy J and Yuan Z 2014 Assessing the spatial and temporal variability of diffusive methane and nitrous oxide emissions from subtropical freshwater reservoirs *Environ. Sci. Technol.* **48** 14499–507

Naselli-Flores L 2003 Man-made lakes in Mediterranean semi-arid climate: the strange case of Dr Deep Lake and Mr Shallow Lake *Hydrobiologia* **506–509** 13–21

R Core Team 2014 *R: A Language and Environment for Statistical Computing* (Vienna: R Foundation for Statistical Computing)

Rasilo T, Prairie Y T and del Giorgio P A 2015 Large-scale patterns in summer diffusive CH4 fluxes across boreal lakes, and contribution to diffusive C emissions *Glob. Change Biol.* **21** 1124–39

Raymond P A *et al* 2013 Global carbon dioxide emissions from inland waters *Nature* **503** 355–9

Samiotis G, Pekridis G, Kaklidis N, Trikoilidou E, Taousanidis N and Amanatidou E 2018 Greenhouse gas emissions from two hydroelectric reservoirs in Mediterranean region *Environ. Monit. Assess.* **190** 363

Schlesinger W H 2009 On the fate of anthropogenic nitrogen *PNAS* **106** 203–8

Schlesinger W H and Bernhardt E S 2013 *Biogeochemistry: An Analysis of Global Change* (New York: Academic)

Schmidt U and Conrad R 1993 Hydrogen, carbon monoxide, and methane dynamics in Lake Constance *Limnol. Oceanogr.* **38** 1214–26

Seitzinger S P, Kroeze C and Styles R V 2000 Global distribution of $N_2O$ emissions from aquatic systems: natural emissions and anthropogenic effects *Chemosphere—Glob. Change Sci.* **2** 267–79

Sepulveda-Jauregui A, Hoyos-Santillan J, Martinez-Cruz K, Walter Anthony K M, Casper P, Belmonte-Izquierdo Y and Thalasso F 2018 Eutrophication exacerbates the impact of climate warming on lake methane emission *Sci. Total Environ.* **636** 411–9

Sierra A, Jiménez-López D, Ortega T, Ponce R, Bellanco M J, Sánchez-Leal R, Gómez-Parra A and Forja J 2017a Distribution of $N_2O$ in the eastern shelf of the Gulf of Cadiz (SW Iberian Peninsula) *Sci. Total Environ.* **593–594** 796–808

Sierra A, Jiménez-López D, Ortega T, Ponce R, Bellanco M J, Sánchez-Leal R, Gómez-Parra A and Forja J 2017b Spatial and seasonal variability of $CH_4$ in the eastern Gulf of Cadiz (SW Iberian Peninsula) *Sci. Total Environ.* **590–591** 695–707

Soued C, del Giorgio P A and Maranger R 2015 Nitrous oxide sinks and emissions in boreal aquatic networks in Québec *Nat. Geosci.* **9** 116

Staehr P A, Bade D, Bogert M C V, de, Koch G R, Williamson C, Hanson P, Cole J J and Kratz T 2010 Lake metabolism and the diel oxygen technique: State of the science *Limnol. Oceanogr. Methods* **8** 628–44

Tang K W, McGinnis D F, Frindte K, Brüchert V and Grossart H-P 2014 Paradox reconsidered: methane oversaturation in well-oxygenated lake waters *Limnol. Oceanogr.* **59** 275–84

Tranvik L J *et al* 2009 Lakes and reservoirs as regulators of carbon cycling and climate *Limnol. Oceanogr.* **54** 2298–314

West W E, Coloso J J and Jones S E 2012 Effects of algal and terrestrial carbon on methane production rates and methanogen community structure in a temperate lake sediment *Freshwater Biol.* **57** 949–55

West W E, Creamer K P and Jones S E 2016 Productivity and depth regulate lake contributions to atmospheric methane: lake productivity fuels methane emissions *Limnol. Oceanogr.* **61** S51–61

Weyhenmeyer G A, Kosten S, Wallin M B, Tranvik L J, Jeppesen E and Roland F 2015 Significant fraction of $CO_2$ emissions from boreal lakes derived from hydrologic inorganic carbon inputs *Nat. Geosci.* **8** 933–6

Wood S N 2006 *Generalized Additive Models: An Introduction with R* (New York: Chapman and Hall/CRC))

Wood S N 2011 Fast stable restricted maximum likelihood and marginal likelihood estimation of semiparametric generalized linear models *J. R. Stat. Soc.* B **73** 3–36

Yvon-Durocher G, Allen A P, Bastviken D, Conrad R, Gudasz C, St-Pierre A, Thanh-Duc N and del Giorgio P A 2014 Methane fluxes show consistent temperature dependence across microbial to ecosystem scales *Nature* **507** 488–91

Zarfl C, Lumsdon A E, Berlekamp J, Tydecks L and Tockner K 2015 A global boom in hydropower dam construction *Aquat. Sci.* **77** 161–70

Zhao Y *et al* 2015 A comparison of methods for the measurement of $CO_2$ and $CH_4$ emissions from surface water reservoirs: Results from an international workshop held at Three Gorges Dam, June 2012 *Limnol. Oceanogr. Methods* **13** 15–29